EUROPEAN JOURNAL OF BIOMEDICAL AND PHARMACEUTICAL SCIENCES
http://www.ejbps.com

ISSN 2349-8870
Volume: 7
Issue: 6
108-117
Year: 2020

# INVESTIGATION OF PROTEIN RESISTANT SURFACES

**[*1]Nidiya Nubia Caleb, [2]Atinga Vallada and [3]Na'acha Frank Emina**

[1]Hospital Services Management Board, PMB 2206, Yola, Adamawa State, Ngeria.
[2]Gombe State University, Faculty of Pharmacy, Gombe, Nigeria.
[3]Department of Zoology, School of Pure and Applied Sciences, Modibbo Adama University of Technology Yola, Adamawa State, Nigeria.

***Corresponding Author: Nidiya Nubia Caleb**
Hospital Services Management Board, PMB 2206, Yola, Adamawa State, Ngeria.

**Article Received on 09/04/2020** **Article Revised on 29/04/2020** **Article Accepted on 20/05/2020**

## ABSTRACT
In this study, we demonstrated the influence of size and shape of the model proteins (fibrinogen and bovine serum albumin) and surface chemistry on poly (KSPMA) brush and methyltriethoxy silane (MTEOS) on gold with respect to the adsorption kinetics. Adsorption profiles was built up for fibrinogen and bovine serum albumin (BSA) at concentrations of 31.2, 62.5, 125, 250, 500 and 1000 µg/mL, through manual injection over a period of 30 seconds for each concentration in that order into a quartz crystal microbalance (QCM) cell on gold, polymer 3-sulfonylpropyl methacarylate (KSPMA) brush and methyl-triethoxy silane (MTEOS). Substrate surfaces where fabricated by plasma enhanced chemical deposition (PECVD) using radiofrequency control at 3W with MTEOS, amino phenyl triethoxy silane (APTES) on QCM gold and Polymerisation of 3-sulfonylpropyl methacarylate (KSPMA) from α-Bromo-isopropyl bromide (BIBB) functionalised with APTES as initiator on gold quartz crystal. The amount of protein adsorbed onto poly (KSPMA) brush and MTEOS films was evaluated with quartz crystal microbalance: BSA was adsorbed more on the polymer (KSPMA) brush than on gold and conversely, fibrinogen was more on gold than the poly (KSPMA) brush. No protein adsorption was observed on MTEOS as result of the film thickness and super-hydrophobicity as seen with decreased frequency and increase bandwidth of the resonance spectra by 16MHz. This work shows that, size and shape of proteins determine their adsorption pattern on substrate surfaces. Also, the thickness of the film coating on the quartz crystal microbalance affects its sensitivity in detecting protein adsorption.

**KEYWORDS:** Protein adsorption, Antifouling, Biomedical device, Biofouling and Surface chemistry.

## 1.0 INTRODUCTION
Protein adsorption and related bio-adhesion is a critical short-coming in micro-fluidics, drug delivery systems and biomedical implants. The rise in the utilisation of medical devices is orchestrated by an aging coupled with advances in medicine.[1] Though this devices improve the quality of life, they are also a risk factor in health associated infections (HAIs) which is defined as infections patients come down with while treating another disease condition.[2] Infections related to indwelling medical devices are three among the five most common HAIs which are surgical site infection, Catheter associated urinary tract infection (CAUTIs), Ventilator-associated pneumonia (VAPs) etc.[2] A review by Neoh *et al.* stated that an estimated 4 million patients acquire HAIs annually based on data from European centre for disease control and prevention (ECDC).[2] National cost statement report of 2017 indicated that HAIs cost NHS £1 billion annually.[3] Also, in a related statistic, nearly $ 9.8. billion is the yearly financial burden incurred by US adult inpatients at acute care hospitals attributable to implantable devices. In the United states alone, approximately a million cases of devices related infection incidence was recorded in 2004 with orthopaedic implants accounting for 4.3% and cardiovascular implants 7.4%.[4,5]

Protein adsorption is the initial step in bio-fouling contamination of surfaces with cells attachment to a pre-adsorbed protein layer before proliferating and spreading Figure1. Such surfaces that demonstrate low protein adsorption are important in many areas, especially parts that cannot be clean for extended period, e.g. boat hulls.[6] Adsorption of protein on biomaterial surfaces is sequentially followed by biofilm, habitation of micro-organism which further develop biofilms. Bio-films on biomedical device surfaces are of significance to public health as the related micro-organisms demonstrates drastic decrease in susceptibility to antimicrobial agents as stated by Donlan.[7] This vulnerability may be as a natural outcome of growth in the biofilm or acquired due

to transfer of extrachromosomal entities to susceptible organisms in the biofilm.[7]

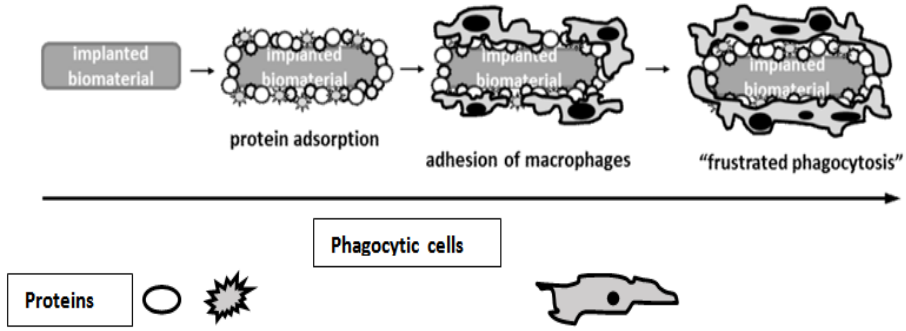


**Figure 1: Human *body response to an implanted biomaterial device.*[10]**

Surface chemistry of biomaterials are patterned to change their physicochemical attributes that dictate their interaction with proteins.[8] It is widely accepted that hydrophilicity promotes protein repellence.[8] Protein resistance is a function of physicochemical properties of the substrate surfaces such as surface chemistry, topography and charge.[8] Surface chemistry can be altered through the application of self-assemble monolayers SAMs in a predictable and reproducible manner. Also, SAMs can be patterned on sensor surfaces such as quartz crystal microbalance (QCM), surface plasmon resonance (SPR) and atomic force microscopy (AFM) to probe protein characteristics on surfaces.[11,12] Limitation comes with the use of SAMs which is the high-level organisation is not a depiction of the natural biomaterial as stated by Dhruv.[11] Also are SAMs are more applicable to gold or silver coated surfaces.[1] A method of imparting functionality that is gaining wide acceptance is the plasma enhanced chemical vapour deposition (PECVD). Apart from being economical, compatibility with wide range of materials it can alter surface chemistry regardless of geometry, therefore, giving room for modification of micro and Nano particles. In addition, it provides an elevated level of surface chemistry regulation during coating. Shen and Zhu described silanes as molecules that bind to a surface but have enough mobility that they can close pack on the surface aided by their specific affinity of the end group, which provides a simple way of manipulating surface properties.[13,14]

## 3.0. MATERIALS AND METHODS

Bovine serum albumin (lyophilized powder), heat shock fraction, pH 7.0 ≥98%, (A7906 Sigma Aldrich), human fibrinogen plasminogen, Von Wilbrand factor (VWF) and fibronectin depleted (FIB 33580 Ab100% clot table Swansea UK Enzyme Research). Phosphate buffered saline (PBS) was freshly prepared dissolving one tablet of Oxoid® BR00014G (Dulbecco A) g/l in 100 ml of distilled water to give pH of 7.3±0.2, NaCl 8.0 mmol; KCl 0.2 mmol; $Na_2HPO_4$ 1.15 mmol; $KClH_2PO_4$ mmol at 25 °C. Protein solutions in the concentration limits of 3.0-1000 µg/ml was prepared immediately before use. Deionised water was used f-or all the experiments.

### 3.0.1. Fabrication of surface

Self-assemble monolayers SAMs can be generated on substrate surfaces when neutral gasses such as helium are ionised (plasma), meets a vaporised chemical in a uniform electromagnetic field, a process called plasma enhanced chemical vapour deposition (PECVD).[16] Chemically treated surfaces were prepared by SAMs of 3-aminopropyl triethoxysilane (APTES), phenltriethoxysilane, (PTEOS), methyltriethoxysilane (MTEOS), trimethoxysilypropyl) diethylenetriamine (DETA), (sigma Aldrich) using atmospheric pressure plasma deposition with Coaxial power® radio frequency control at 3watts and plasma pen distance from the substrate surface was 2 mm to mimic hydrophobic and hydrophilic surfaces, separately on gold quartz crystal. The helium gas was bubbled into the bubbler bottle to generate vaporised silane which reacts with the plasma to produce self-assembled monolayers of the silane.

### 3.0.2. Deposition of α-Bromo isopropyl bromide (BIBB) onto APTES-Functionalized Gold Quartz crystal

APTES functionalised QCM gold was placed in a dry glass petri dish. To trigger amide initiator, dry tetra hydro-furan THF, Sigma Aldrich,10 mL and 2-bromoisobutyryl bromide (BIBB,>98%,0.26 mL,0.48 g,2.10 mmol into the glass petri dish containing the APTES treated gold quartz crystal. After the gold quartz 5hrs crystal was taken out and rinsed with THF, Methanol, and distilled water and was dried with stream of air.

### 3.0.3 Polymerisation of 3-sulfonylpropyl methacarylate (KSPMA) from BIBB functionalised gold quartz crystal

The 3-sulfopropyl methacrylate potassium salt (1.012 g, 70.2 mmol, Sigma was dissolved in methanol: distilled water (2:1 vol/vol), d.$H_2O$ was 21 mL in total (14ml of $CH_3OH$ and 7ml $H_2O$), which was stirred and degassed by bubbling through $N_2$ for 20 min in a 100 mL, sealed three round bottom flasks. After 10 min, all the monomer was dissolved and 2,2'-bipyridyne (bpy, 0.651 g, 4.17 mmol, Sigma Aldrich) and (CuCl 0.0179 g) and ($CuCl_2$,0.08 mmol, sigma Aldrich) were added. The mixture was stired and degassed for an hour.

Subsequently, copper (1) bromide (CuBr, 99.9%, 02.30 g, 1.6 mmol, Sigma Aldrich) was added. The gold crystal was dipped in the polymer solution, sealed and was left to stay for 24hrs.

### 3.0.4 Wettability test

In determining absorption kinetics and level of proteins that can adsorb to a substrate surface, surface energy becomes a critical factor. Water contact angle is used to assess surface wettability based on the tendency of the water droplet to advance (hydrophilic) or to remain (hydrophobic).[17] Substrate surface with water contact angle ($C_{AW}$) of >90° is termed hydrophobic (high wettability) whereas it is defined as hydrophilic (low wettability) for $C_{AW}$ < 90°[18] Figure 2 . From the perspective of wetting energetics, hydrophilic surface wettability expends greater than 1.3 kj/mol of surface-sites and hydrophobic surface wetting take up less than 1.3 kj/mol of surface-sites.[17] In terms of H-bonding surrounding the water molecule involved in the wetting interaction, hydrophilic surfaces wet with > one H-bond per water molecule, conversely, hydrophobic surface utilise < one hydrogen bond per water molecule. Drop shape analysis was carried out using One Attention Theta Lite Biolin scientific to confirm the deposition of hydrophobic or hydrophilic silanes with a 5µL syringe. It was also used to check the deposition of α-Bromoisopropyl bromide (BIBB) onto APTES-Functionalized gold quartz crystal and polymerisation of 3-sulfonylpropyl methacarylate (KSPMA).

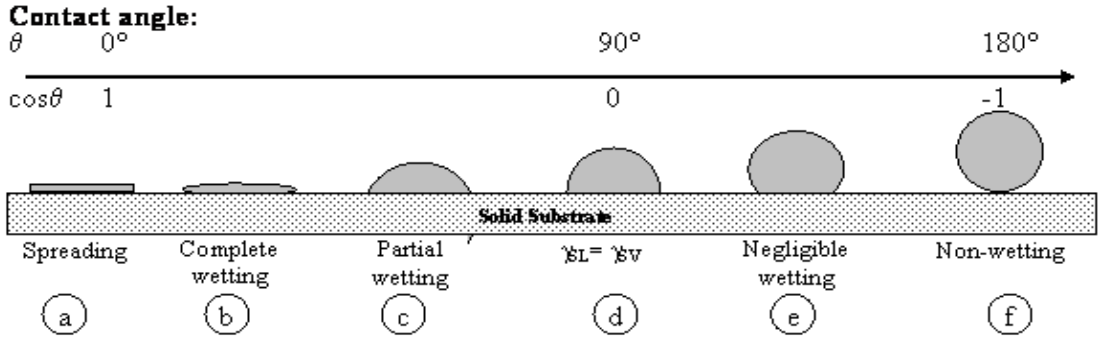


**Figure 2: Wettability scale of 0-180° on a substrate surface. The schematic above shows different degrees of surface wettability a-f.[19]**

### 3.0.5. Quartz crystal microbalance

Measurements from quartz crystal microbalance were obtained using Novatech® Open QCM 1.2 M2|01-0.1-1815 MT.10 MHz, 4.42^-9 $cm^{-2}$, AT-fundamental, Frequency tolerance of ±20 kHz at 23ºC, resistance of <10 Ω Au-titanium substrate, blank diameter 13.9 mm and electrode diameter 6 mm.

QCM measures sensor works based on piezoelectric characteristics of the crystal. Mechanical vibrations are generated when alternating current is applied. QCM measures the change in frequency in relation to the mass variation on its surface. A quartz crystal can be sensitive to as low as 0.1 $ngcm^{-2}$. Measurements are very precise, thus, a highly sensitive analytical device.[20] Sauebrey *et al* explored the chances of quartz crystal resonator devices for quantitative estimation of mass.[21] The added mass of the deposited film was discovered to be proportional to the frequency shift of a thickness shear vibrating quartz crystal resonator.[21]

$$\Delta F = \frac{f_q^2 M_f}{N\rho_q S} = -\frac{f_q^2 m_f}{N\rho_q} \qquad Equation\ [1]$$

Where $f_{q\,=}$ is the fundamental resonant frequency of the Quartz, N is the frequency constant of the specific crystal cut ($N_{AT}$ =1.67^5 HZ .cm; $N_{BT}$ = 2.5^5 Hz.cm), $\rho_q$ =2.65 $kg/dm^3$ is the quartz density, $S$=is the surface area of the deposited film and the mass $M_f$. Sohna and Cooper, establishes that there is strong correlation between change in mass per unit area and QCM signals for peptides and proteins in liquid solution based on the equation 1.[21]

1mL soft-ject® syringe was used to pump 0.5 mL blank of phosphate buffer solution into the QCM tubes through a control tap and was left to equilibrate for an hr. The experiment was optimised through slow injection of the blank, slight bending of the delivery tube backwards to avoid air reading on the QCM sensor during liquid change as well minimal shock around the QCM was ensured. Following this, 0.3 mL of varying concentrations (31.2, 62.5, 125, 250, 500 and 1000 µg/mL) solutions of Fibrinogen. was injected over a period of 30 seconds for each concentration in that order after. The quartz crystal was washed in PBS once then distilled water and ethanol alternatively 3 times and finally, in propanol once. It was left to dry for 1 hr. The experiment was repeated this time using BSA.

### 3.1. FTIR-ATR

Infra-red analysis of the surface adhered protein was carried out using a Thermo scientific Nicolet iN10 MX FTIR spectrophotometer with Omnic picta operating software, steadily purged with dry air. Attenuated total reflectance mode was used by fitting in the Germanium crystal. Fourier transform infrared spectroscopy-attenuated total reflectance involves directing light directing infra-red light at junction between a prism with

high refractive index called the internal reflection element (IRE). e.g. diamond, silicon or germanium. The angle of the incidence of IR beam exceeds the critical angle, hence total internal reflection. A standing wave (evanescent wave) is established at the reflective surface which interacts with the sample attenuating the light beam leaving the IRE. The ATR-FTIR is basically a surface technique since the evanescent wave only interacts with a several micrometre layers thickness of the sample, it is of benefit in protein studies and easy sample preparation.[22] In modern spectroscopy of proteins, FTIR-ATR is undoubtedly a powerful tool that is label free, non-destructive that can provide a sensitive insi-tu analysis across a broad system. FTIR-ATR was used to further establish the deposition of the plasma enhanced vaporised silanes, model proteins on the plasma silane treated surfaces, α-bromoisobutyryl bromide (BIBB) and poly (KSPMA) on QCM gold.

Proteins with considerable differences in properties were selected for this study. Serum albumin is the most abundant plasma protein in the vertebrates, synthesized in the liver as precursor (pre-proalbumin) before it is processed further to maturity and release into circulation. It has a heart-shaped structures with various domains[23], with a unique presence of 17 disulphide bridges providing high protein stability and extra-ordinary binding properties. It is an established fact that bovine serum albumin has high similarity to human serum albumin in sequence and conformity. Also, it is cheap and accessible.[24]

### 3.1.1. Model protein under investigation: Bovine serum albumin (BSA) and Fibrinogen

Fibrinogen (Fg), a soluble glycoprotein present in the blood at the concentration of 2.5-4.0 mg/mL.[26] with mass of 340 kDa. It is an essential component of coagulation cascade being a precursor of fibrin.[27] Data based on x-ray electron microscopy and crystallography revealed that Fibrinogen molecule possess rod-like shape of 45 nm in length and~ 2-3 nm in diameter. Each molecule is characterised by 2 distant and one middle globular part linked by 17 nm triple and partially quadruple α-helical coils made up of S-S bonds Fig. 2. Also, is the unordered part from the extreme coiled-coiled of αA chain termed α-C domains making up about ¼ of the mass of the molecule. The two regions of α-C associate with each other at the central region.[26]

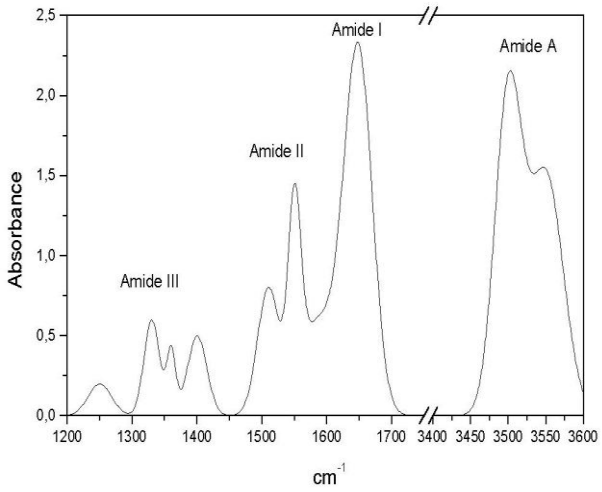


**Figure 3: Schematic sample of protein spectra with amide band I, II and III.[19]**

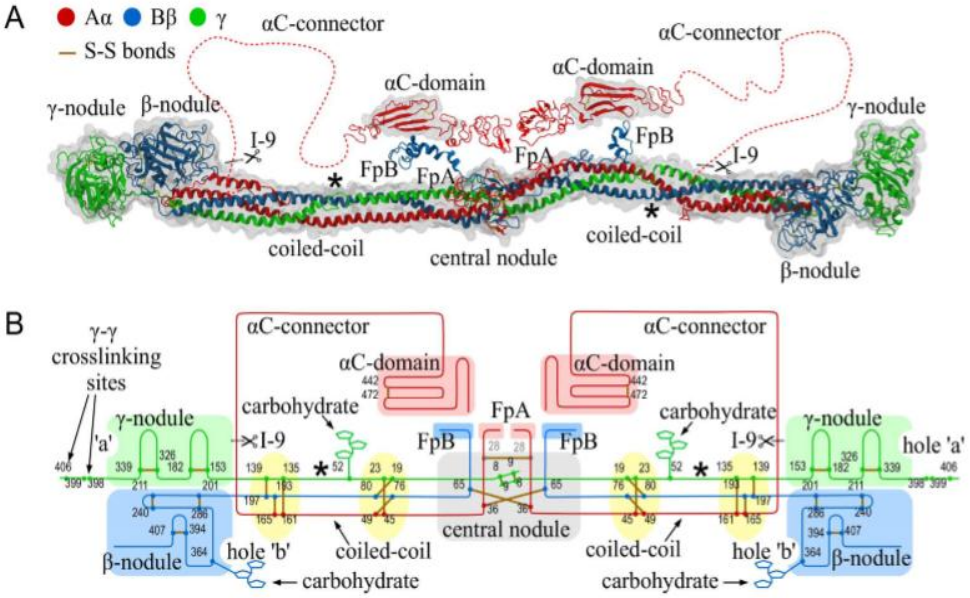


**Figure 4: Structure of human Fibrinogen.[A] Detailed structure showing the nodles and other parts.[B] a schematic of fibrinogen in its native form.**

## 4.0 RESULTS AND DISCUSSION

### 4.1. Drop Shape Analysis

**Table 1: Silanes used, initiator (BIBB) polymer brush and their wettability on gold with static water contact angle of mean average of six measurements.**

| Exposure time | Power | Distance | Treatment | Wettability | | |
|---|---|---|---|---|---|---|
| | | | | $C_{AW}$ | | Control |
| 5 secs | 3w | 2 mm | APTES-BIBB | 60.1° | 10.2º | Glass |
| | | | POLYMER | 24.7° | 60.1° | APTES-BIBB |
| 5 secs | 3w | 2mm | MTEOS | 60.1° | 10.1° | Glass |

Thin polymeric brush film of KSPMA on QCM gold was characterised using a drop shape before and after deposition of BIBB. The mean static contact angle measurements confirmed the successful formation of polymer on the substrate surface Figure 7. The polymer brush film coated surface was more hydrophilic than the BIBB: the static contact angle decline from 60.1 ° to 24.7°. because of the Zwitterionic groups along the polymer chains. This confers upon the surface electrical neutrality, a requirement for protein repellent surface. The results obtained agree with the work carried out by Cho *et al.*

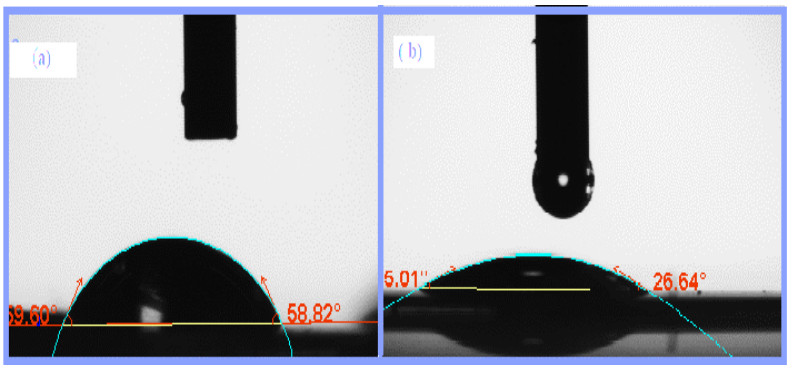


**Figure 5: Static water contact angles of (a) SAMs of BIBB (initiator) and (b) (KSPMA) polymer brush film.**

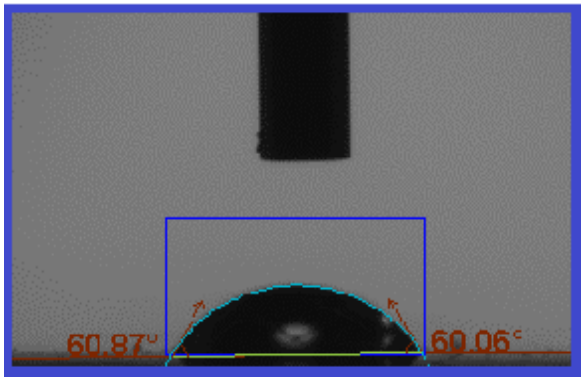


**Figure 6. Static Water contact angle of MTEOS on gold.**

#### 4.1.1. FTIR-ATR analysis

**Table 2: Spectral wave bands, regions and vibrational modes of BSA protein on QCM gold.**

| Wave band $cm^{-1}$ | Region | Vibrations |
|---|---|---|
| 1662 | Amide band I | C=O |
| 1574 | Amide band II | N-H bending |
| 3309 | Amide A band | N-H stretch |

The above spectra in Figure 3. shows amide band I and II tallying with wave bands 1662 $cm^{-1}$ (C=O) stretch and 1574 $cm^{-1}$ N-H bending vibrations of the wave bands while 3309 is the amide A band due to N-H stretch.

**Table 3: Spectral wave bands and vibrational Modes of the initiator (BIBB) on QCM gold.**

| Wave band $cm^{-1}$ | Vibrations |
|---|---|
| 1659 | C=O stretching |
| 1466 | $-CH_2$ bending |
| 115 | C-O stretching |

The formation of the initiator (BIBB) from the APTES functionalised surface on gold was confirmed by FTIR spectroscopy showing characteristic peaks as presented in Table 3. above.

**Table 4: FTIR spectral wave bands and vibrational modes of Poly (KSPMA) brush film and MTEOS on gold.**

| Wave band $cm^{-1}$ | Vibrations |
|---|---|
| 3407 | N-H Stretching |
| 1727 | C=O Stretching |
| 1580 | N-H stretching |
| 1456 | N-H bending |
| 1417 | Quaternary ammonium |
| 1211 | S=O asymmetric |
| 1041 | S=O symmetric |
| 1069 | Si-O |

The formation of the poly (KSPMA) on the gold surface was further confirmed also by FTIR which shows characteristic peaks as well as the plasma enhanced chemical deposition of MTEOS on gold summarised in Table 4.

### 4.1.2 Protein adsorption

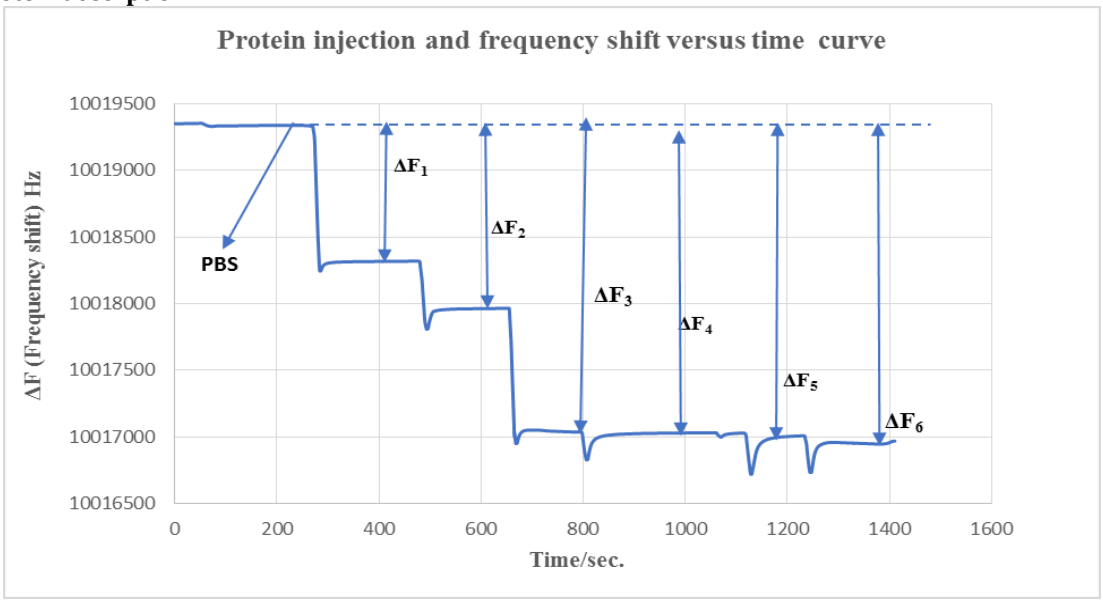


**Figure 7: Shows points of injection with PBS as the blank then correspondingly with the frequency shift are the various protein concentrations [31.25, 62.5, 125, 250, 500 and 1000 µg/mL] injection.**

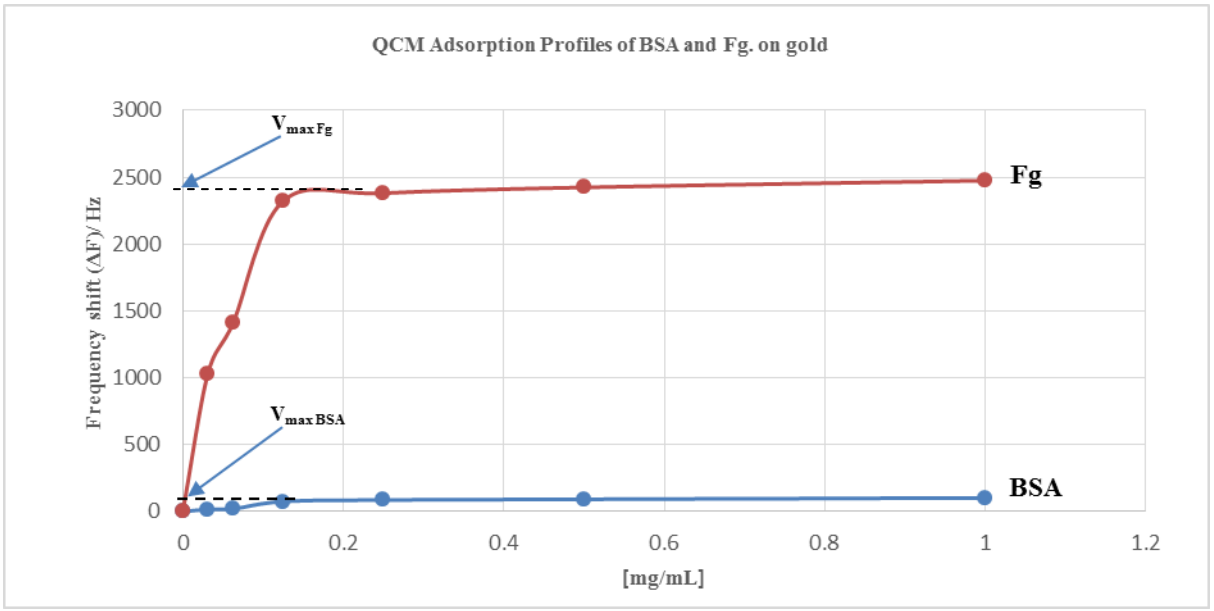


**Figure 8: Showing the absorption profile of Fibrinogen with a very steep gradient and bovine serum albumin nearly flat on gold.**

Higher frequency shift (ΔF) and a larger $V_{max}$ was observed with fibrinogen due to its high Mwt. 340 kDa (maximum binding i.e., larger Vmax) and fibrinogen has steeper initial gradient (slope) due to higher binding capacity (stronger strength of binding 'K').[25] In the contrast, BSA has lower frequency shift with lower Mwt. of 66.4 kDa. Also, smaller initial gradient is indicative of weaker binding (low 'K'). Moreover, highly elongated and flexible fibrinogen molecule demonstrates higher frequency shift at this concentration because of its size, stickiness and rod-like shape. At such high concentration, the rod-like molecules rearrange to increase protein-protein interaction as well as surface concentration of the protein[25] Fig.12

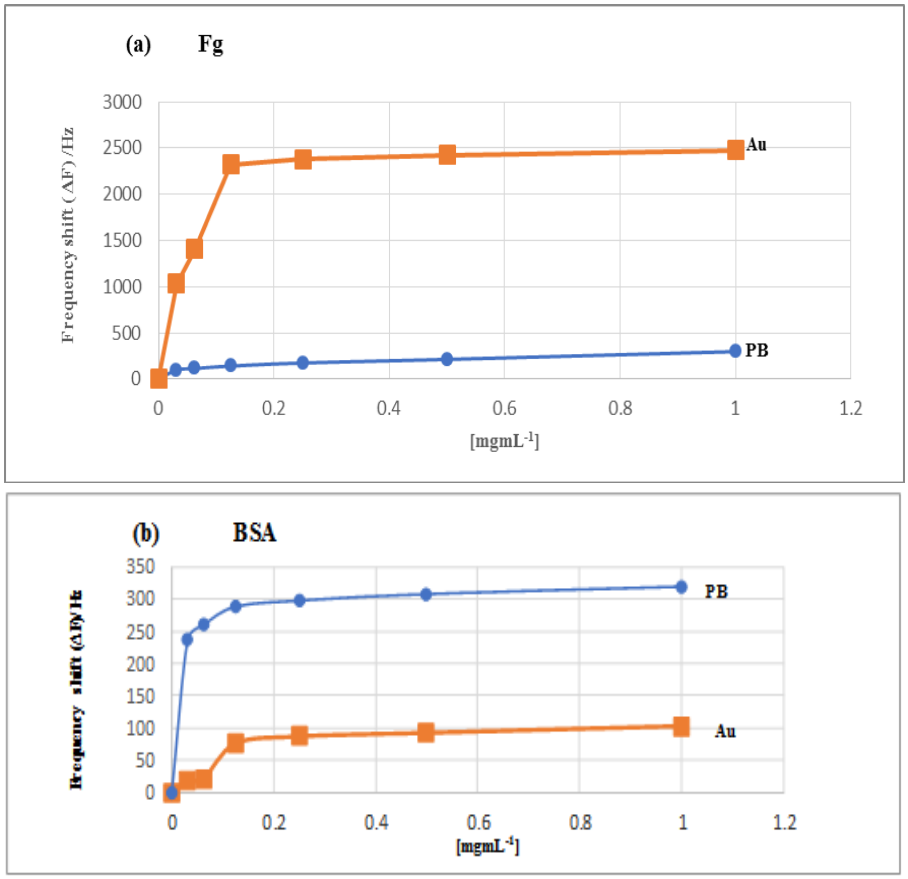


**Figure 9: Absorption profiles of (a) Fibrinogen and (b) BSA on QCM gold (Au) and polymer brush (Pb). Initial stock concentration was 1 mg mL$^{-1}$.**

Larger $V_{max}$ and a higher frequency shift were observed with adsorption of Fibrinogen on gold compared to the polymer brush as seen Figure 9a. This can possibly be linked to the rod-like shape of the fibrinogen molecule which on the flat gold surface undergoes molecular rearrangement to accommodate more molecules at an elevated concentration[25] but on the polymer brush, the broad shaped nature of the fibrinogen molecule limits its level of adsorption between brush bristle thus lower frequency shift and smaller $V_{max}$. Reverse is the case with globular and smaller size albumin, where higher frequency shifts and larger $V_{max}$ was recorded on the polymer brush compared to the gold surface Figure 9b. This can be attributed to the size and shape of the protein molecule which is small enough to occupy more spaces in between the polymer brush, whereas on gold the adsorption in any orientation would result in almost uniform surface coverage.[25] This follows interpretation of protein adsorption according to the work of Roach *et al.*[25]

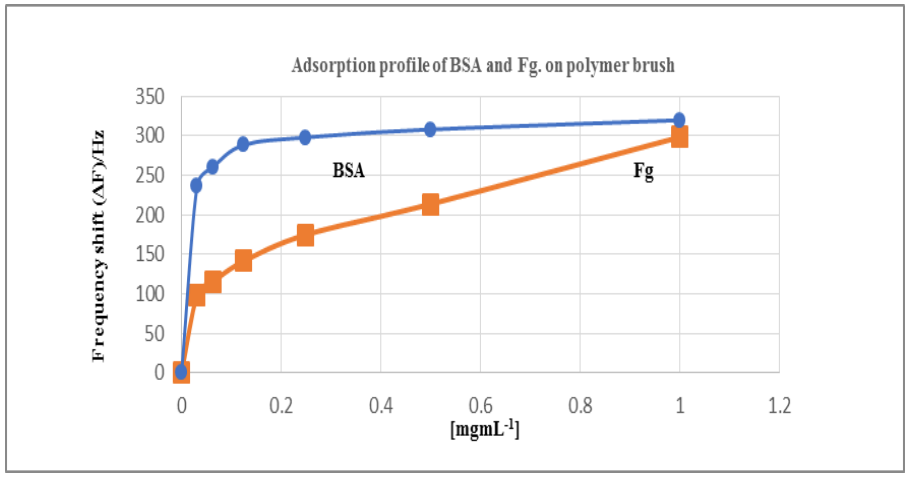


**Figure 10: Adsorption profile of BSA and Fibrinogen on polymer brush showing BSA with larger Vmax compared to Fg.**

**4.1.3. Protein adsorption on 3-sulfonylpropyl methacarylate (KSPMA) polymer brush.**

KSPMA polymer brush falls under the class of Zwitterionic protein repellent surface, because it is hydrophilic and electrically neutral. Furthermore, phospholipids from the cell membrane are zwitterionic in nature, therefore materials synthesize based on this concept may be biocompatible.[28] In this work, we fabricated protein repellent surfaces by depositing BIBB on to APTES-functionalised quartz crystal gold to form thin polymeric brush film.

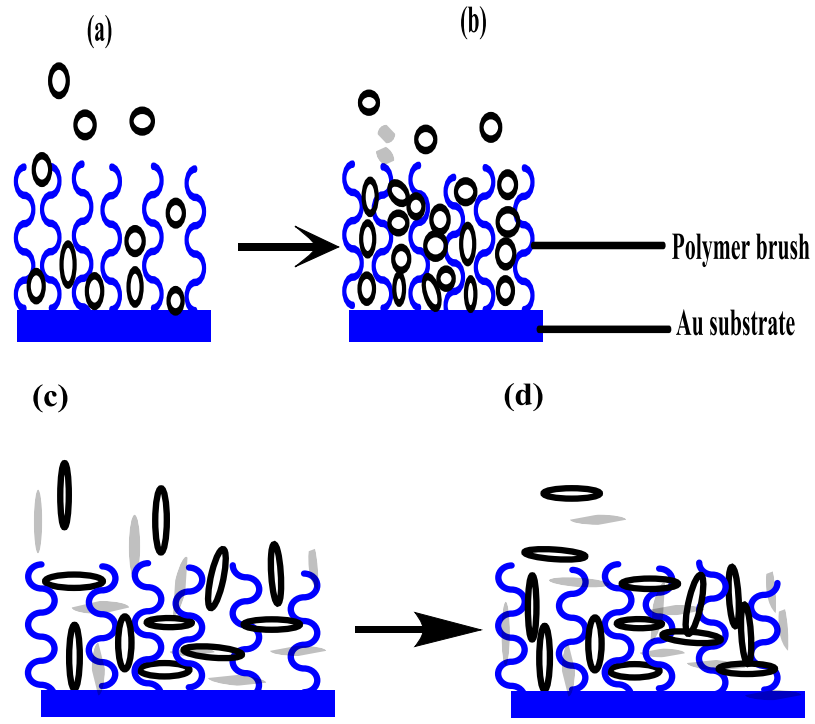


**Figure 11: Schematic of BSA molecule and Fibrinogen molecule adsorption onto polymer brush at low (a)/(c) and high (b)/(d) concentration.**

The polymer brush, Figure 11a and 11b accommodates a greater number of the oval shaped and smaller size BSA molecules until maximum concentration is reached at saturation where no available space is left in between the brush bristles. On the contrary, the rod-like shape fibrinogen, fewer molecules are adsorbed unto the brush surfaces because of its shape and size which possibly prevents it from taking more spaces between the brush bristles, Figure11c and 11d.

**4.1.4. Protein adsorption on MTEOS coated Quartz crystal gold**

Protein adsorption profile for MTEOS on QCM gold did not work as expected, however, this is likely to explains the failure, that the MTEOS layer on the quartz crystal was probably too thick which caused the frequency shift to be above the fundamental frequency (overtone at 16MHz) Figure 12. There by resulting into what Luan *et al*. called "hearing loss". This can possibly be that the sensor can no longer pick any vibrations from the crystal because the MTEOS film was too thick. Secondly, the hydrophobic nature of MTEOS is likely to be the cause, however on exposure to the plasma oxygen, silanol groups develop at the expense of the methyl groups on the surface layer. The silanol groups are polar in nature, consequently making the exposed surface hydrophilic as observed with the low value of static water contact angle, Figure 8, above.[29] This is well elaborated by Roach *et al*. study on decoupling of the liquid response of a super hydrophobic quartz crystal microbalance, which suggest that such surface repels liquid flow on the crystal surface as seen in Figure 10 with increase band width frequency, a concept called interfacial slip.[30]

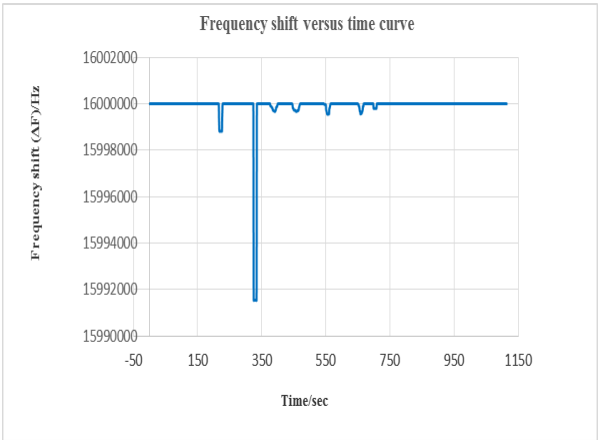


**Figure 12: *QCM profile of protein on MTEOS coated quartz gold illustrating increase in bandwidth frequency of 16 MHz.***

## 5.0 CONCLUSION

In summary, the QCM adsorption profile shows that the shape and size of adsorbing protein molecule determines the pattern of protein repellences on substrate surfaces. Higher frequency shift of 233.2 MHz with larger Vmax. was observed with Fibrinogen on gold when compared to BSA on the same substrate with smaller frequency shift (62.5Hz) and Vmax. These differences can be linked to the fact that the big size, stickiness and rod like-shape of Fibrinogen. Also, the protein-protein interaction as well as the surface concentration is increased as the rod-like molecules of Fg. re-arrange at peak concentration.

Stepper initial concentration gradient and a higher frequency shift 232.2Hz was observed with gold when compared to polymer brush. The rod-like shape of Fibrinogen molecules undergoes molecular rearrangement on the gold substrate in order to accommodate more molecules of Fg at high concentration which possibly accounts for the observation. Conversely, on the polymer brush the broad shaped nature of Fg. limits its extent of adsorption within the brush bristle, consequently lower frequency shift of 115.2Hz and smaller Vmax was recorded. Contrastingly, the globular and small size BSA recorded a high frequency shift of 288.5 Hz and a larger Vmax on the polymer brush when compared to gold surfaces which has a lower frequency shift (75.8Hz) and a smaller initial concentration gradient. The size and shape of the BSA which is small enough to take up more spaces within the brush bristles, whereas on gold the adsorption in any direction would result in almost the same surface coverage. MTEOS recorded 16MHz which is above the fundamental frequency (overtone). This is probably due to the thickness of the MTEOS on the QCM that led to what is called “hearing loss”. The QCM sensor can no longer pick vibrational waves because the MTEOS film appears to be thicker than needed.

Following these observations, it can be deduced that the gold surfaces repels more of BSA than Fg. while the polymer brush adsorbs more BSA than Fg. attributable to the differences in size and shape of the adsorbing proteins. The concept of size and shape can be considered as a factor that determines the extent of protein adsorption on substrate surfaces. This should be put into consideration when tailoring protein repellent surfaces.

## ACKNOWLEDGEMENT

I would like to extend my deep gratitude to my supervisor, a great teacher, Dr. Paul Roach, for giving me the enabling environment to learn under him and work in his laboratory. My appreciation goes to the team members; Dr. Munya K and Dan Merryweather, Loughborough university and the chemistry department Loughborough university.

I am thankful to all my colleagues in the chemistry department Loughborough university for their warm friendship and PTDF (Petroleum Development Trust Fund) for financial support.

Lastly, I would like to thank my siblings for their support, Justin B. Nidiya, and my uncles especially those who made it possible for me to be here.

## REFERENCES

1. Thevenot T, Hu W, Tang L. Surface Chemistry Influences Implant Biocompatibility. *Curr Top Med Chem*, 2008; 8(4): 270–280.
2. Neoh KG, Li M, Kang ET, Chiong E and Tambyah PA. Surface Modification Strategies for Combating Catheter-Related Complications: Recent Advances and Challenges. *J. Mater. Chem. B*, 2017; 21; 5(11): 2045–2067.
3. National Institute for Health and Care Excellence. *Infection : prevention and control of healthcare-associated infections in primary and community care.partial update of NICE Clinical guidelines 2*, London: Royal College of Physicians, 2017.
4. Hetrick EM and Schoenfisch MH. Reducing Implant-Related Infection: Active Release Strategies. Chem Soc Rev., 2006; 35(9): 780–789.
5. Dutta SS, Chatterjee S, Maiti PK. Evaluation of the Role Substrate and Albumin on Pseudomonas aeruginosa Biofilm Morphology through FESEM and FTIR Studies on Polymeric Biomaterials. *Prog Biomater*, 2017; 6: 27 - 38.
6. Koc Y, de Mello AJ, McHale G, Newton MI, Roach P and Shirtcliffe NJ. Nano-scale superhydrophobicity: suppression of Protein Adsorption and Promotion of Flow-induced detachment. *Lab on a Chip*, 2008; 8: 582.
7. Donlan RM. Biofilm Formation: A Clinically Relevant Microbiological Process *Clin. Infect. Dis.*, 2001; 33(8): 1387–1392.
8. Liascukiene I, El Kirat K, Beauvais M, Asadauskas SJ, Lambert JF and J. Landoulsi J. Lipid Layers on Nanoscale Surface Topography: Stability and Effect on Protein Adsorption. *Langmuir*, 2017; 33(18): 4414–4425.
9. Zhang H and Chiao M. Anti-fouling Coating of Poly (dimethylsiloxane) Devices for Biomedical Applications. *J. Med. Biol. Eng.*, 2015; 35(2): 143–155.
10. Utrata-Wesoek A. *Polimery/Polymers*, 2013; 58: 685–695.
11. Dhruv DH. Surface Engineering of Polymeric Biomaterials. Utah State University, 2009.
12. Rufin MA, Barry ME, Adair PA, Hawkins ML, Raymond JE and Grunlan MA. P rotein Resistance Efficacy of PEO-Silane Amphiphiles: Dependence on PEO-Segment Length and Concentration. *Acta Biomater.*, 2016; 41: 247–252.
13. Shen L and Zhu J. Heterogeneous Surfaces to Repel Protein. *Adv. Colloid Interface Sci.*, 2016; 228: 40–54.
14. Arkles B. Hydrophobicity, Hydrophilicity and Silane Surface Modification, Gelest,Inc.,

Morrisville, 2006.
15. Yochelis S, Katzir E, Kalcheim Y, Gutkin V, Millo O and Paltiel Y. Formation of Au-Silane Bonds. *Journal of Nanotechnology*, 2012; 2012.
16. Dimitrakellis P and Evangelos G. Hydrophobic and Superhydrophobic surfaces Fabricated Using Atmospheric Pressure and Cold Plasma Technology: A Review. *Advance in Colloid and Interface Science*, 2018; 254: 1–21.
17. Xu LC, Bauer JW and Siedlecki CA. Proteins, Platelets and Blood Coagulation at Biomaterial Interfaces. *Colloids Surfaces B Biointerfaces*, 2014; 124: 49–68.
18. Yuan Y and Lee TR. *Contact Angle and Wetting Properties*, Springer Series in Surface Sciences, Berlin Heidelberg, 51st edn., 2013.
19. http://lejpt.academicdirect.org/A10/029_038_files/image001.gif (accessed 06/09/2017)
20. https://plus.google.com/+Openqcm_Quartz_Crystal_Microbalance (accessed *25/07/2017)*.
21. Sohna JES and Cooper MA. Does the Sauerbrey Equation Hold True for Binding of Peptides and Globular Proteins to a QCM? A Systematic Study of Mass Dependence of Peptide and Protein Binding with a Piezoelectric Sensor. *Sens. Bio Sens. Res.*, 2016; 11: 71–77.
22. Glassford SE, Byrne B and Kazarian SG. Recent Application of ATR FTIR Spectroscopy and Imaging to Protein. *Biochem. Biophys Acta - Proteins Proteomics*, 2013; 1834(12): 2849–2858.
23. Huang BX, Kim H and Dass C. Probing Three-Dimentional Structure of Bovine Serum Albumin by Chemical Cross-Linking and Mass Spectrometry. *Am. Soc. Mass Spectrom.*, 2004; 15(8): 1237–1247.
24. Lacobucci C, Gotze M,and Ihling CH. A Cross-Link/Mass Spectrometry Workflow Based on MS-Cleavable Cross-Linkers and the MeroX Software for Studying Protein Structures and Protein-Protein Interactions. *Nat. Protoc.*, 2018; 13(12): 2864-2889.
25. Roach P, Farrar D and Perry CC. Interpretation of Protein Adsorption: Surface-Induced Conformational Changes. *J. Am. Chem. Soc.*, 2005; 127(22): 8168–8173.
26. Zuev YF, Litvinov RI, Sitnitsky AE, Idiyatullin BZ, Bakirova R, Galanakis D, Zhmurov A, Barsegov V and Weisel JW. Conformational Flexibility and Self-Association of Fibrinogen in Concentrated Solutions. *J. Phys. Chem.*, 2017; 121(33): 7833-7843.
27. Kamath S and Lip GYH. Fibrinogen: Biochemistry, Epidemiology and Determinants. *Q J Med.*, 2003; 96(10): 711–729.
28. Cho WK, Kong B and Choi IS. Highly Efficient Non-Biofouling Coating of Zwitterionic Polymers: Poly ((3-Methacryloylamino) Dimethyl (3-Sulfopropyl) Ammonium Hydroxide). *Langmuir*, 2007; 23(10): 5678–5682.
29. Bhattacharya S, Datta A, Berg JM and Gangopadhyay S. Studies on Surface Wettability of Poly(Dimethyl) Siloxane(PDMS) and Glass Under Oxygen-Plasma Treatment and Correlation with Bond Strength. *J. Microelectromechanical Syst.*, 2005; 14(3): 590–597.
30. Roach P, Mchale G, Evans CR, Shirtcliffe NJ and Newton MI. Decoupling of the Liquid Response of a Superhydrophobic Quartz Crystal, Microbalance. *Langmuir*, 2007; 23(19): 9823–9830.